Thickness-dependent electronic band structure in MBE-grown hexagonal InTe films

A. V. Matetskiy [1,2,*] V. V. Mararov [1] A. N. Mihalyuk [1,3,†] N. V. Denisov [1]
S. V. Eremeev [4] A. V. Zotov [1] and A. A. Saranin [1]

[1]*Institute of Automation and Control Processes, Far Eastern Branch of the RAS, Vladivostok 690041, Russian Federation*
[2]*Istituto di Struttura della Materia, Consiglio Nazionale delle Ricerche, Trieste I-34149, Italy*
[3]*Institute of High Technologies and Advanced Materials, Far Eastern Federal University, 690950 Vladivostok, Russia*
[4]*Institute of Strength Physics and Materials Science SB RAS, 634021 Tomsk, Russia*

Films of the hexagonal InTe with thicknesses from one to three tetralayers (TLs) were synthesized on the bilayer graphene/SiC by molecular beam epitaxy. Valence bands of the one- and two-TL-thick films were found to be flat-like near $\bar{\Gamma}$ point, but become parabolic for the three-TL-thick film and beyond. The band gap of the InTe was found to be equal to 2.1 eV for the single tetralayer and tends to reduce its size with thickness. The band structure calculations revealed a large spin splitting of the InTe single tetralayer lower conduction band with exclusive out-of-plane spin polarization. Bearing in mind inaccessibility of the hexagonal InTe in a bulk form, all above-mentioned findings open up a way for the further study of this perspective material.

I. INTRODUCTION

Layered chalcogenides provide a rich playground for a variety of condensed matter topics [1], such as semiconductor technologies [2], topological insulators [3], and superconductors [4]. Recent interest to the two-dimensional (2D) materials in a context of green technologies, spintronics, and valleytronics pushes these materials even higher, as their quasi-2D nature provides an opportunity to isolate or grow individual layers that will remain stable. Absence of dangling bonds on the surface of these materials not only makes them relatively stable towards ambient conditions but also opens up a way for stacking of various functional layers in a controlled manner in order to construct artificial heterostructure with desired properties [5]. While electron band structure of the layered chalcogenides has an almost 2D character, it still depends on thickness, especially in an ultrathin region. Thus the III-VI materials (e.g., InSe, InS, and GaSe) were found to exhibit valence band shape transition from the bulk-like parabolic one to a Mexican-hat-like shape [6–9].

The III-VI materials were found to be perspective for use in solar energy conversion [10,11], field-effect transistors [12], broadband photodetection [11,13], photocatalysis [14,15], and thermoelectricity [16]. The band gap of these materials was found to strongly vary under applied field [17,18] that can be used in electronics and optoelectronics. The peculiar Mexican-hat-like dispersion of the ultrathin films provides 1D-like electronic density of states at the valence band edge [7]. In turn, a corresponding large number of conducting modes can enhance the thermoelectric properties [16,19]. Moreover, such sharp van Hove singularity near the

Fermi level could lead to an exchange splitting of the electronic states and associated tunable magnetism [20]. From the spintronic point of view, the III-VI materials were found to be promising in the tasks of the optical spin pumping [21], spin transfer [22], and spin-current generation [23].

While the ultrathin layers of hexagonal InSe and GaSe were successively synthesized and corresponding valence band shape transition was observed directly [24,25], the hexagonal phase of the InTe and GaTe appears to be less favorable than the monoclinic one. However, it was found that the hexagonal phase of GaTe can be realized in the thin films and flakes [26,27]. In the present paper, we report on the synthesis of the ultrathin hexagonal InTe film on bilayer graphene substrate by a molecular beam epitaxy (MBE) approach. We explored the changes in the electronic structure as a function of film thickness starting from a single tetralayer, using angle-resolved photoemission spectroscopy (ARPES), scanning tunneling spectroscopy (STS), and *ab initio* calculations. We found that similar to InSe, the hexagonal InTe exhibits transition from the almost flat Mexican-hat-like shape of the valence band at one- and two-layer-thick samples to the parabolic shape at the higher thicknesses. We also presented detailed spin-resolved analysis of the InTe single TL electronic structure, in particular, peculiar spin texture of a conduction band valley in $\bar{M}$ point.

II. EXPERIMENTAL AND CALCULATION DETAILS

MBE growth of InTe films was conducted in the ultrahigh vacuum (UHV) chamber with a base pressure less than 5.0×10^{-10} Torr, equipped with a reflection-high-energy electron diffraction (RHEED) facility. The bilayer graphene (BLG) was used as a substrate. It was formed by direct-current annealing at 1300 °C of the 6H-SiC wafer. The BLG substrate was chosen instead of a monolayer graphene due to

*mateckij@iacp.dvo.ru
†mih-alexey@yandex.ru

165301-1

the better surface quality and robustness of the self-limited growth procedure. Indium and tellurium were deposited from the Knudsen cells heated to 750 °C and 300 °C, respectively, while the substrate was kept at 400 °C, which led to the InTe growth rate of 0.06 tetralayer/min. Higher or lower Te:In flux ratios lead to change of the RHEED pattern from a streaky to a spotty one that we attributed to indium telluride phases of different stoichiometry, albeit without studying them due to their bad morphology. Thus parameter space for the InTe growth appears to be similar to the case of the kindred InSe compound [28]. The prepared InTe/BLG/SiC samples were transferred into the Scienta Omicron UHV chamber equipped with ARPES and low energy electron diffraction (LEED) or into the Unisoku LT-STM UHV chamber. Transportation was done using an evacuated transfer unit without breaking the vacuum. ARPES measurements were conducted using a VG Scienta R3000 electron analyzer and high-flux He discharge lamp ($h\nu = 21.2$ eV). Scanning tunneling microscopy and spectroscopy (STM and STS) measurements were conducted with the PtIr tip.

Density functional theory (DFT) calculations were performed using Vienna *ab initio* simulation package [29,30], with core electrons represented by projector augmented wave (PAW) potentials [31]. The generalized gradient approximation [32] to the exchange-correlation functional was used. For estimation of charge transfer the Bader atomic charges [33] were calculated. The van der Waals interaction was implemented using the DFT-D2 scheme [34]. In order to increase the accuracy of band structure calculations we used the Heyd-Scuseria-Ernzerhof screened hybrid functional [35] with spin-orbit coupling taken into account. The kinetic cutoff energy was 400 eV and $10 \times 10 \times 1 k$-point mesh was used to sample the InTe/BLG surface Brillouin zone (SBZ).

III. RESULTS AND DISCUSSION

The ball-and-stick model of the hexagonal InTe tetralayer (TL) placed on BLG is shown in Fig. 1(a). The in-plane lattice constant of the InTe coincides with the graphene $\sqrt{3}$ lattice distance (4.26 Å). We use this $\sqrt{3} \times \sqrt{3}$ graphene cell for the DFT calculations. Previous calculations predicted similar values for the InTe lattice constant within the range of 4.24–4.39 Å [6,36]. Due to the fact that $\mathbf{a}_{InTe}$ is close to $\sqrt{3}\mathbf{a}_{gr}$, the majority of the InTe nucleation islands appears to be rotated by 30° with respect to the substrate. As a result, InTe film tends to be single crystalline, which can be seen in the LEED pattern in Fig. 1(b). However, the grains with alternative orientations are also present at the chosen growth parameters.

According to the STM observations, the islands of InTe have a triangular shape with the terrace size of up to 200 nm [Fig. 1(c)]. As follows from the STM profile, the height of the terrace step is close to 0.9 nm [Fig. 1(d)], which coincides with the calculated values for the graphene-TL distance of 0.923 nm and TL-TL distance of 0.874 nm. The atomically resolved STM image shows a well-ordered hexagonal pattern [Fig. 1(e)]. It is noteworthy that films are quite homogeneous but not absolutely uniform in respect to thickness [see large-scale STM image in Fig. 1(c)]. However, we were still able to trace evolution of the band structure with thickness.
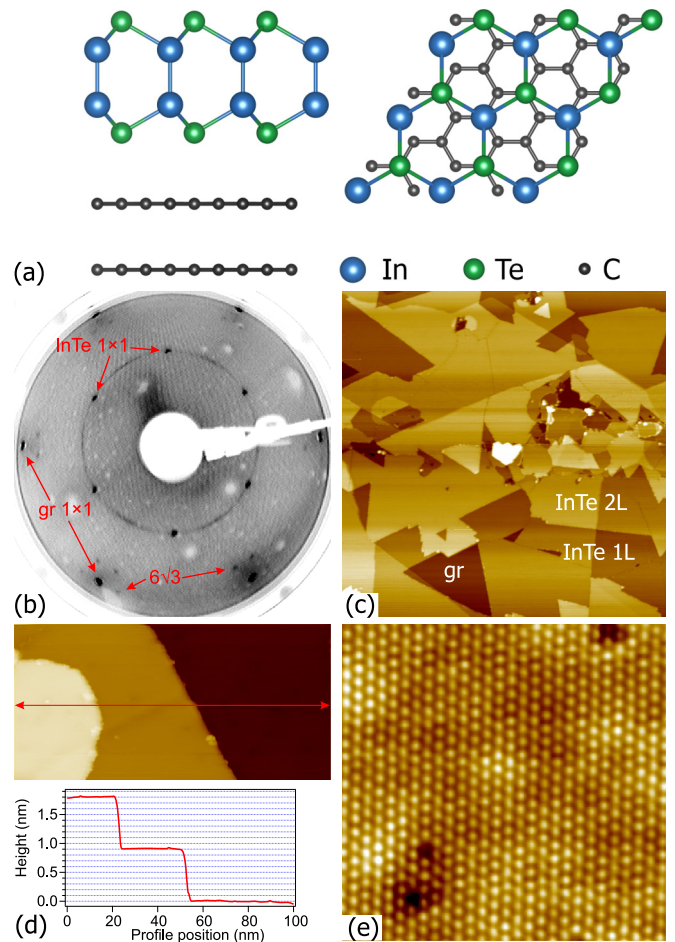

FIG. 1. (a) Side and top views for the ball-and-stick model of the InTe single TL placed atop BLG. (b) LEED pattern of the InTe film grown on BLG. Most of the InTe islands are aligned at 30° to the graphene lattice. However, islands with other alignments also exist that lead to appearance of the corresponding ring in the LEED pattern. (c) Typical large-scale STM image (500×500 nm^2, V$_s = 2$ V, $I = 150$ pA) of the InTe few-TL film grown on the BLG. (d) STM image (100×50 nm^2, V$_s = 2$ V, $I = 100$ pA) of the InTe steps together with corresponding steps profile along the red line. (e) Atomic-scale STM image (10×10 nm^2, V$_s = -1.9$ V, $I = 150$ pA) of the InTe single tetralayer.

Figures 2(b)–2(d) show ARPES spectra for InTe films with thicknesses varied from 1 TL to 3 TL (here the number of layers corresponds to the most prevalent one for the corresponding sample). Similar to the InSe and GaSe [24,25] materials, the band structure of InTe strongly depends on the thickness. The one- and two-TL-thick films have a flat shape of the upper valence band (UVB) near the $\bar{\Gamma}$ point. The flatlike shape is especially pronounced in the case of single TL where electron energy stays constant for almost half of the BZ [see Fig. S1(a) in the Supplemental Material [37] for momentum dependence of the energy distribution curves]. The UVB is formed mostly by Te and In p_z orbitals [Figs. 3(a) and 3(b)]. Due to a strong interlayer coupling of p_z orbitals, stacking of additional layers leads to the splitting of the UVB of individual TL and transition from the Mexican-hat-like shape to the parabolic one for the films with thickness of three TL
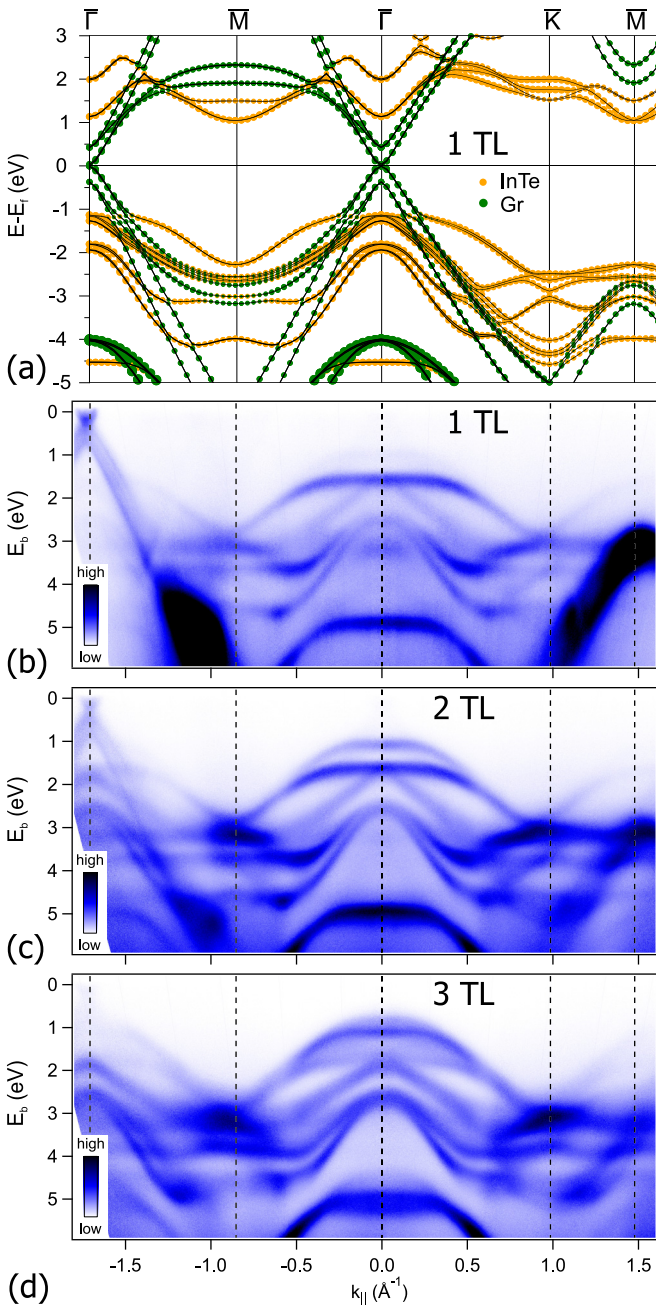
FIG. 2. (a) Layer-projected band structure calculated for the InTe single TL on BLG. Green and yellow colors depict graphene and InTe states, respectively. (b)–(d) Evolution of the band dispersion of the InTe film with thickness obtained by ARPES. The crystallographic directions in (a) and (b)–(d) are the same. For the ARPES spectra of one (b) and two (c) TL, the bands of the uncovered BLG may be seen at $\bar{\Gamma}_1$ and at $\bar{K}$-$\bar{M}$-$\bar{K}$ areas.

and higher. In calculated bulk spectrum this leads to the quite sizable bandwidth of the UVB in k_z direction of 1 eV (see Fig. S2) [37].

In turn, the experimental ARPES data for the single TL of InTe shown in Fig. 2(b) is in a good agreement with the DFT calculations presented in Fig. 2(a) and with the prediction for the free-standing InTe [6]. The same is true for the case of experimental and calculated InTe spectra of higher

thicknesses (see Fig. S1 [37]). However, we did not observe a strong replica of the BLG π bands in the $\bar{\Gamma}$ point, which arises in the calculations of structure ordered within the $\sqrt{3} \times \sqrt{3}$ unit cell. There is also no sign of anticrossing of InTe valence bands with such a π band replica. Moreover, DFT Bader charge transfer calculation predicts the transfer of only 0.006 e from InTe to the graphene, which also indicates that InTe film is indeed decoupled from the supporting substrate. These observations imply that interaction of the InTe with graphene is negligible and calculations may even overestimate it. For example, there is a prediction that in the InTe-graphene heterostructure the gap of 36 meV may arise in the Dirac point [38], but our observations do not support that. Let us examine details of the electronic and spin structure of one-TL InTe film adsorbed on BL graphene. Figures 3(a) and 3(b) show the orbital-resolved relativistic spectrum, where one may see that the lower conduction S1 band is formed mainly by In s and Te p_z orbitals and the upper valence S2 band is mainly formed by In and Te p_z orbitals. Deeper valence bands approaching S2 in the $\bar{\Gamma}$ point are mainly formed by $p_{x,y}$ orbitals. Atomic spin-orbit coupling (SOC) leads to the relatively strong splitting of these bands, lifting their degeneracy at the $\bar{\Gamma}$ point [see inset in Fig. 3(a)]. This splitting value Δ is equal to 680 meV for both bands, which is almost twice greater than in the case of InSe single layer [21].

Spin-resolved relativistic spectrum in Fig. 3(c) demonstrates that both S1 and S2 bands have dominating out-of-plane spin polarization, especially away from the $\bar{\Gamma}$ point. Thus Fig. 3(d) displaying the volumetric representation of the S1 spin split band and its spin texture shows the exclusive dominance of $S_{\bar{z}}$ spin component with a large spin splitting along the $\bar{K}$-$\bar{M}$-$\bar{K}$ direction. In contrast, the S1 band and other bands stay degenerate in the $\bar{\Gamma}$-$\bar{M}$ direction due to symmetry constraint. Hexagonal InTe has a mirror plane that is perpendicular to the xy plane and lies along $\bar{\Gamma}$-$\bar{M}$. This leads to a zero orbital angular moment for corresponding k vectors and a nonzero away from $\bar{\Gamma}$-$\bar{M}$. Similar symmetry constraints keep the valence band of monolayer TMD degenerate in the $\bar{\Gamma}$-$\bar{M}$ direction, while valleys in $\bar{K}$ points exhibit strong spin splitting [39–41].

It is worth noting that these spin-polarized states of the S1 band around the $\bar{M}$ point lie 90 meV lower of its own degenerate dispersion in the vicinity of the $\bar{\Gamma}$ point. Such a separation of the nondegenerate conduction band from the other adjacent bands over the entire $k_\parallel$ space of the SBZ makes the system promising for spintronic applications. Thus, for the InSe family, $\sigma^{+/-}$-polarized light may selectively excite valence band electrons into spin up/down states in the conduction band [21]. This process should be even more efficient for the InTe due to the heavier chalcogen nucleus. There is also a proposal of the use of InSe family monolayers in a charge-to-spin conversion device as the top valence band has a tiny splitting in the $\bar{\Gamma}$-$\bar{K}$ direction [22,23]. Our calculation results also show such splitting for the InTe monolayer [Fig. 3(b)]; however, it is difficult to distinguish it in the ARPES as the amount of splitting is below the experimental resolution of our setup. Despite the fact that both valence band and conduction bands are away from the Fermi level one may use various approaches to access them such as doping [42], defect engineering [43], application of an electric field [44], or strain [45]. Finally, we
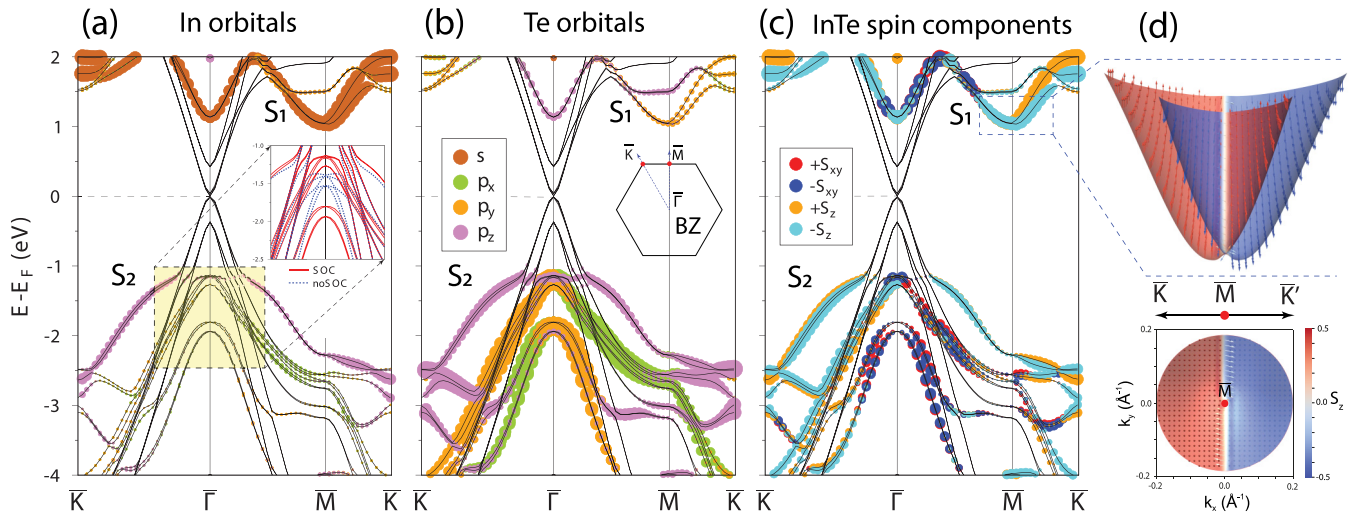
FIG. 3. (a), (b) In and Te orbital-projected relativistic spectra, respectively (the orbital characters of the bands are shown by brown, green, orange, and violet colors for s, p_x, p_y, and p_z orbitals, respectively). Inset in (a) shows an effect of the SOC on the light hole bands formed by $p_{x,y}$ orbitals in $\bar{\Gamma}$ point. (c) Spin-polarized relativistic spectrum (where red and dark blue balls correspond to the respective in-plane spin components and orange and light blue balls to the out-of-plane ones). In all panels, the symbol size corresponds to the magnitude of the respective orbital/spin components. All spectra are calculated along the high-symmetry directions of the SBZ, shown in the inset of panel (b). (d) Enlarged volumetric visualization of S1 lower conduction band in a side and top view and associated spin texture.

studied the band gap of InTe films using the STS method. According to the STS measurements, the band gap of a single TL is equal to 2.1 eV [Fig. 4(a)], which finds a consistency with our DFT calculations predicting the same gap value of 2.1 eV [Fig. 2(a) and Fig. 4(b)]. For the two-TL-thick film, the gap reduces to 1.8 eV, as follows from STS observation shown in Fig. 4(a) and DFT calculations shown in Fig. S2(c) [37]. Such an interplay between the thickness and gap size was already mentioned for many layered chalcogenides [46–48]. In the case of the InSe-type materials, this trend mostly reflects the expansion of the UVB bandwidth at the $\bar{\Gamma}$ point with thickness.

IV. CONCLUSION

In conclusion, the hexagonal InTe was synthesized in a form of ultrathin films. The transition of the valence band shape from the Mexican-hat-like one in the one- and two-TL-thick films to the parabolic one for the higher thicknesses was observed directly by the ARPES and confirmed by DFT calculations. It was shown that with increasing number of InTe tetralayers, as more Te p_z states interact through interlayer coupling, the bandwidth increases and the top point of the UVB at $\bar{\Gamma}$ moves to higher energy. Associated decrease of the band gap with thickness was proved by the STS measurements. DFT calculations revealed large spin splitting of the electronic bands with exclusive out-of-plane spin polarization at the bottom of the conduction band, which makes the synthesized material promising for further spin-transport studies. Bearing in mind that the hexagonal InTe is the heaviest one among the InSe-type materials, all possible spintronic applications, already reported for this family [21–23], may be more effective in the case of InTe.
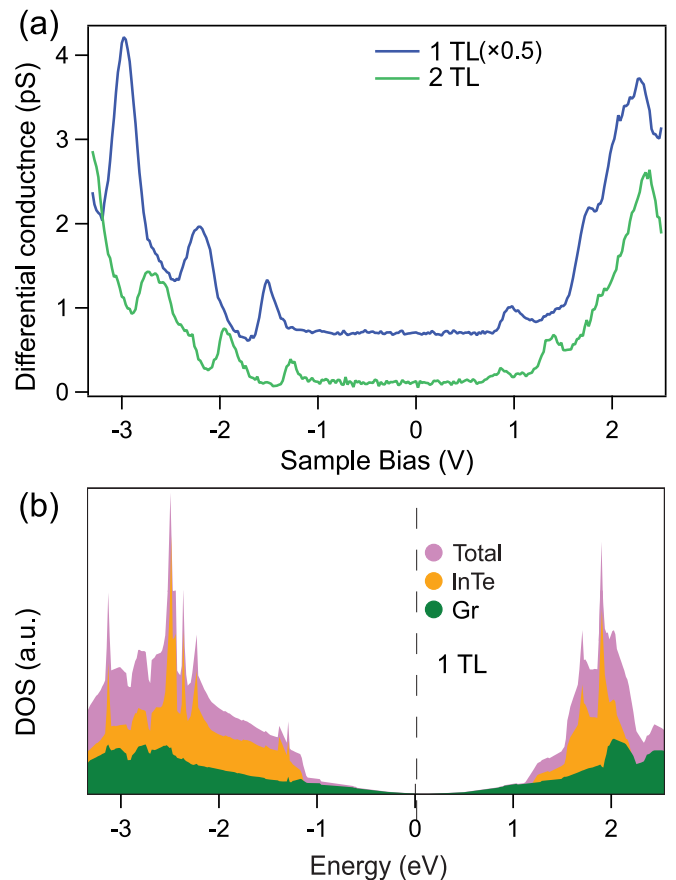

FIG. 4. (a) STS measurements taken from the InTe islands of different thicknesses. $I_{setpoint} = 100$ pA, $V_{setpoint} = -2.7$ V, lock-in amplitude $= 20$ mV, and frequency $= 983$ Hz. (b) Calculated DOS for the InTe single TL on BLG.

[1] N. Briggs, S. Subramanian, Z. Lin, X. Li, X. Zhang, K. Zhang, K. Xiao, D. Geohegan, R. Wallace, L. Q. Chen, M. Terrones, A. Ebrahimi, S. Das, J. Redwing, C. Hinkle, K. Momeni, A. Van Duin, V. Crespi, S. Kar, and J. A. Robinson, A roadmap for electronic grade 2D materials, 2D Mater. **6**, 022001 (2019).

[2] B. Radisavljevic, A. Radenovic, J. Brivio, V. Giacometti, and A. Kis, Single-layer MoS_2 transistors, Nat. Nanotechnol. **6**, 147 (2011).

[3] H. Zhang, C.-X. Liu, X.-L. Qi, X. Dai, Z. Fang, and S.-C. Zhang, Topological insulators in Bi_2Se_3, Bi_2Te_3 and Sb_2Te_3 with a single Dirac cone on the surface, Nat. Phys. **5**, 438 (2009).

[4] S. Tan, Y. Zhang, M. Xia, Z. Ye, F. Chen, X. Xie, R. Peng, D. Xu, Q. Fan, H. Xu, J. Jiang, T. Zhang, X. Lai, T. Xiang, J. Hu, B. Xie, and D. Feng, Interface-induced superconductivity and strain-dependent spin density waves in $FeSe/SrTiO_3$ thin films, Nat. Mater. **12**, 634 (2013).

[5] A. K. Geim and I. V. Grigorieva, Van der Waals heterostructures, Nature (London) **499**, 419 (2013).

[6] V. Zólyomi, N. D. Drummond, and V. I. Fal'ko, Electrons and phonons in single layers of hexagonal indium chalcogenides from *ab initio* calculations, Phys. Rev. B **89**, 205416 (2014).

[7] D. V. Rybkovskiy, A. V. Osadchy, and E. D. Obraztsova, Transition from parabolic to ring-shaped valence band maximum in few-layer GaS, GaSe, and InSe, Phys. Rev. B **90**, 235302 (2014).

[8] V. Zólyomi, N. D. Drummond, and V. I. Fal'ko, Band structure and optical transitions in atomic layers of hexagonal gallium chalcogenides, Phys. Rev. B **87**, 195403 (2013).

[9] C. Sun, H. Xiang, B. Xu, Y. Xia, J. Yin, and Z. Liu, *Ab initio* study of carrier mobility of few-layer InSe, Appl. Phys. Express **9**, 035203 (2016).

[10] J. Martínez-Pastor, A. Segura, J. L. Valdes, and A. Chevy, Electrical and photovoltaic properties of indium-tin-oxide/p-InSe/Au solar-cells, J. Appl. Phys. **62**, 1477 (1987).

[11] S. R. Tamalampudi, Y.-Y. Lu, R. Kumar U., R. Sankar, C.-D. Liao, K. Moorthy B., C.-H. Cheng, F. C. Chou, and Y.-T. Chen, High performance and Bendable few-layered InSe photodetectors with broad spectral response, Nano Lett. **14**, 2800 (2014).

[12] W. Feng, W. Zheng, W. Cao, and P. Hu, Back gated multilayer InSe transistors with enhanced carrier mobilities via the suppression of carrier scattering from a dielectric interface, Adv. Mater. **26**, 6587 (2014).

[13] S. Lei, L. Ge, S. Najmaei, A. George, R. Kappera, J. Lou, M. Chhowalla, H. Yamaguchi, G. Gupta, R. Vajtai, A. D. Mohite, and P. M. Ajayan, Evolution of the electronic band structure and efficient photo-detection in atomic layers of InSe, ACS Nano **8**, 1263 (2014).

[14] Q. Peng, R. Xiong, B. Sa, J. Zhou, C. Wen, B. Wu, M. Anpo, and Z. Sun, Computational mining of photocatalysts for water splitting hydrogen production: Two-dimensional InSe-family monolayers, Catal. Sci. Technol. **7**, 2744 (2017).

[15] C. Wen, Z. Zhang, Z. Guo, J. Shen, B. Sa, P. Lin, J. Zhou, and Z. Sun, Two-dimensional O-phase group III monochalcogenides for photocatalytic water splitting, J. Phys.: Condens. Matter **32**, 065501 (2020).

[16] D. Wickramaratne, F. Zahid, and R. K. Lake, Electronic and thermoelectric properties of van der Waals materials with ring-shaped valence bands, J. Appl. Phys. **118**, 075101 (2015).

[17] L. Debbichi, O. Eriksson, and S. Lebègue, Two-Dimensional Indium Selenides Compounds: An *ab Initio* Study, J. Phys. Chem. Lett. **6**, 3098 (2015).

[18] Z. Zhang, Z. Chen, M. Bouaziz, C. Giorgetti, H. Yi, J. Avila, B. Tian, A. Shukla, L. Perfetti, D. Fan, Y. Li, and A. Bendounan, Direct observation of band gap renormalization in layered indium selenide, ACS Nano **13**, 13486 (2019).

[19] J. P. Heremans, V. Jovovic, E. S. Toberer, A. Saramat, K. Kurosaki, A. Charoenphakdee, S. Yamanaka, and G. J. Snyder, Enhancement of thermoelectric efficiency in PbTe by distortion of the electronic density of states, Science **321**, 554 (2008).

[20] T. Cao, Z. Li, and S. G. Louie, Tunable Magnetism and Half-Metallicity in Hole-Doped Monolayer GaSe, Phys. Rev. Lett. **114**, 236602 (2015).

[21] S. J. Magorrian, V. Zólyomi, and V. I. Fal'ko, Spin-orbit coupling, optical transitions, and spin pumping in monolayer and few-layer InSe, Phys. Rev. B **96**, 195428 (2017).

[22] D. T. Do, S. D. Mahanti, and C. W. Lai, Spin splitting in 2D monochalcogenide semiconductors, Sci. Rep. **5**, 17044 (2015).

[23] M. Zhou, S. Yu, W. Yang, W. K. Lou, F. Cheng, D. Zhang, and K. Chang, Current-induced spin polarization in monolayer InSe, Phys. Rev. B **100**, 245409 (2019).

[24] I. A. Kibirev, A. V. Matetskiy, A. V. Zotov, and A. A. Saranin, Thickness-Dependent Transition of the Valence Band Shape from Parabolic to Mexican-hat-like in the MBE Grown InSe Ultrathin Films, Appl. Phys. Lett. **112**, 191602 (2018).

[25] Z. Ben Aziza, D. Pierucci, H. Henck, M. G. Silly, C. David, M. Yoon, F. Sirotti, K. Xiao, M. Eddrief, J.-C. Girard, and A. Ouerghi, Tunable quasiparticle band gap in few-layer GaSe/graphene van der Waals heterostructures, Phys. Rev. B **96**, 035407 (2017).

[26] C. J. Bae, J. McMahon, H. Detz, G. Strasser, J. Park, E. Einarsson, and D. B. Eason, Influence of thickness on crystallinity in wafer-scale GaTe nanolayers grown by molecular beam epitaxy, AIP Adv. **7**, 035113 (2017).

[27] Q. Zhao, T. Wang, Y. Miao, F. Ma, Y. Xie, X. Ma, Y. Gu, J. Li, J. He, B. Chen, S. Xi, L. Xu, H. Zhen, Z. Yin, J. Ren, and W. Jie, Thickness-induced structural phase transformation of layered gallium telluride, Phys. Chem. Chem. Phys. **18**, 18719 (2016).

[28] L. Brahim-Otsmane, J.-Y. Emery, and M. Eddrief, X-ray, reflection high electron energy diffraction and x-ray photoelectron spectroscopy studies of InSe and γ-In_2Se_3 thin films grown by molecular beam deposition, Thin Solid Films **237**, 291 (1994).

[29] G. Kresse and J. Hafner, *Ab initio* molecular dynamics for open-shell transition metals, Phys. Rev. B **48**, 13115 (1993).

[30] G. Kresse and J. Furthmüller, Efficient iterative schemes for *ab initio* total-energy calculations using a plane-wave basis set, Phys. Rev. B **54**, 11169 (1996).

[31] P. E. Blöchl, Projector augmented-wave method, Phys. Rev. B **50**, 17953 (1994).

[32] J. P. Perdew, K. Burke, and M. Ernzerhof, Generalized Gradient Approximation Made Simple, Phys. Rev. Lett. **77**, 3865 (1996).

[33] W. Tang, E. Sanville, and G. Henkelman, A grid-based Bader analysis algorithm without lattice bias, J. Phys.: Condens. Matter **21**, 084204 (2009).

[34] S. Grimme, J. Antony, S. Ehrlich, and H. Krieg, A consistent and accurate *ab initio* parametrization of density functional dispersion correction (DFT-D) for the 94 elements H-Pu, J. Chem. Phys. **132**, 154104 (2010).

[35] A. V. Krukau, O. A. Vydrov, A. F. Izmaylov, and G. E. Scuseria, Influence of the exchange screening parameter on the performance of screened hybrid functionals, J. Chem. Phys. **125**, 224106 (2006).

[36] M. S. Li, K. X. Chen, D. C. Mo, and S. S. Lyu, Predicted high thermoelectric performance in a two-dimensional indium telluride monolayer and its dependence on strain, Phys. Chem. Chem. Phys. **21**, 24695 (2019).

[37] See Supplemental Material at http://link.aps.org/supplemental/10.1103/PhysRevB.106.165301 for additional details on InTe band structure evolution with thickness.

[38] H. Li, Z. Zhou, and H. Wang, Tunable Schottky barrier in InTe/graphene van der Waals heterostructure, Nanotechnology **31**, 335201 (2020).

[39] S. Oh and H. J. Choi, Orbital angular momentum analysis for giant spin splitting in solids and nanostructures, Sci. Rep. **7**, 1 (2017).

[40] K. Komider, J. W. González, and J. Fernández-Rossier, Large spin splitting in the conduction band of transition metal dichalcogenide monolayers, Phys. Rev. B **88**, 245436 (2013).

[41] R. Roldán, M. P. López-Sancho, F. Guinea, E. Cappelluti, J. A. Silva-Guillén, and P. Ordejón, Momentum dependence of spin-orbit interaction effects in single-layer and multi-layer transition metal dichalcogenides, 2D Mater. **1**, 034003 (2014).

[42] D. Wang, X.-B. Li, and H.-B. Sun, Modulation doping: A strategy for 2D materials electronics, Nano Lett. **21**, 6298 (2021).

[43] A. Bafekry, S. Farjami Shayesteh, M. Ghergherehchi, and F. M. Peeters, Tuning the bandgap and introducing magnetism into monolayer BC_3 by strain/defect engineering and adatom/molecule adsorption, J. Appl. Phys. **126**, 144304 (2019).

[44] A. Bafekry, M. Ghergherehchi, and S. Farjami Shayesteh, Tuning the electronic and magnetic properties of antimonene nanosheets via point defects and external fields: First-principles calculations, Phys. Chem. Chem. Phys. **21**, 10552 (2019).

[45] A. S. Rodin, A. Carvalho, and A. H. Castro Neto, Strain-Induced Gap Modification in Black Phosphorus, Phys. Rev. Lett. **112**, 176801 (2014).

[46] G. W. Mudd, S. A. Svatek, T. Ren, A. Patanè, O. Makarovsky, L. Eaves, P. H. Beton, Z. D. Kovalyuk, G. V. Lashkarev, Z. R. Kudrynskyi, and A. I. Dmitriev, Tuning the bandgap of exfoliated InSe nanosheets by quantum confinement, Adv. Mater. **25**, 5714 (2013).

[47] E. P. Mukhokosi, S. B. Krupanidhi, and K. K. Nanda, Band gap engineering of hexagonal $SnSe_2$ nanostructured thin films for infra-red photodetection, Sci. Rep. **7**, 15215 (2017).

[48] Y. Zhang, K. He, C.-Z. Chang, C.-L. Song, L.-L. Wang, X. Chen, J.-F. Jia, Z. Fang, X. Dai, W.-Y. Shan, S.-Q. Shen, Q. Niu, X.-L. Qi, S.-C. Zhang, X.-C. Ma, and Q.-K. Xue, Crossover of the three-dimensional topological insulator Bi_2Se_3 to the two-dimensional limit, Nat. Phys. **6**, 584 (2010).

[49] https://cc.dvo.ru